OXFORD

human reproduction

Human Reproduction, 2024, **39(9),** 2053–2066

https://doi.org/10.1093/humrep/deae154

Advance Access Publication Date: July 16, 2024

Original Article

Reproductive biology

Granulosa cell metabolism at ovulation correlates with oocyte competence and is disrupted by obesity and aging

Atsushi Morimoto[1,2], Ryan D. Rose[1,3], Kirsten M. Smith[1], Doan T. Dinh[1], Takashi Umehara[1,4], Yasmyn E. Winstanley[1], Hiroaki Shibahara[2], Darryl L. Russell[1], and Rebecca L. Robker[1,*]

[1]Robinson Research Institute, School of Biomedicine, University of Adelaide, Adelaide, SA, Australia
[2]Department of Obstetrics and Gynecology, School of Medicine, Hyogo Medical University, Hyogo, Japan
[3]Genea Fertility SA, Adelaide, SA, Australia
[4]Graduate School of Integrated Sciences for Life, Hiroshima University, Hiroshima, Japan

*Correspondence address. Robinson Research Institute, School of Biomedicine, University of Adelaide, Adelaide Health and Medical Sciences Building, Level 5, Adelaide, SA 5005, Australia; E-mail: rebecca.robker@adelaide.edu.au https://orcid.org/0000-0002-1538-4604

ABSTRACT

STUDY QUESTION: Is oocyte developmental competence associated with changes in granulosa cell (GC) metabolism?

SUMMARY ANSWER: GC metabolism is regulated by the LH surge, altered by obesity and reproductive aging, and, in women, specific metabolic profiles are associated with failed fertilization versus increased blastocyst development.

WHAT IS KNOWN ALREADY: The cellular environment in which an oocyte matures is critical to its future developmental competence. Metabolism is emerging as a potentially important factor; however, relative energy production profiles between GCs and cumulus cells and their use of differential substrates under normal *in vivo* ovulatory conditions are not well understood.

STUDY DESIGN, SIZE, DURATION: This study identified metabolic and substrate utilization profiles within ovarian cells in response to the LH surge, using mouse models and GCs of women undergoing gonadotropin-induced oocyte aspiration followed by IVF/ICSI.

PARTICIPANTS/MATERIALS, SETTING, METHODS: To comprehensively assess follicular energy metabolism, we used real-time metabolic analysis (Seahorse XFe96) to map energy metabolism dynamics (mitochondrial respiration, glycolysis, and fatty acid oxidation) in mouse GCs and cumulus–oocyte complexes (COCs) across a detailed time course in the lead up to ovulation. In parallel, the metabolic profile of GCs was measured in a cohort of 85 women undergoing IVF/ICSI ($n = 21$ with normal ovarian function; $n = 64$ with ovarian infertility) and correlated with clinical parameters and cycle outcomes.

MAIN RESULTS AND THE ROLE OF CHANCE: Our study reveals dynamic changes in GC energy metabolism in response to ovulatory LH, with mitochondrial respiration and glycolysis differentially affected by obesity versus aging, in both mice and women. High respiration in GCs is associated with failed fertilization ($P < 0.05$) in a subset of women, while glycolytic reserve and mitochondrial ATP production are correlated with on-time development at Day 3 ($P < 0.05$) and blastocyst formation ($P < 0.01$) respectively. These data provide new insights into the cellular mechanisms of infertility, by uncovering significant associations between metabolism within the ovarian follicle and oocyte developmental competence.

LIMITATIONS, REASONS FOR CAUTION: A larger prospective study is needed before the metabolic markers that were positively and negatively associated with oocyte quality can be used clinically to predict embryo outcomes.

WIDER IMPLICATIONS OF THE FINDINGS: This study offers new insights into the importance of GC metabolism for subsequent embryonic development and highlights the potential for therapeutic strategies focused on optimizing mitochondrial metabolism to support embryonic development.

STUDY FUNDING/COMPETING INTEREST(S): National Health and Medical Research Council (Australia). The authors have no competing interests.

TRIAL REGISTRATION NUMBER: N/A.

Keywords: aging / obesity / mitochondria / glycolysis / granulosa cells / cumulus–oocyte complex / ovulation / metabolism / ovary / IVF/ICSI outcome

Introduction

Oocytes mature in ovarian follicles through an intimate interaction with the surrounding somatic cells, which integrate environmental information such as nutritional, endocrine, and immune signals. These follicular inputs are critical for the acquisition of oocyte developmental competence: the future capacity of the oocyte to undergo fertilization, blastocyst formation, and implantation. Understanding the mechanisms by which the

Received: November 18, 2023. **Revised:** June 16, 2024. **Editorial decision:** June 24, 2024.

surrounding somatic cells influence oocyte developmental competence potentiates the identification of clinical predictors of fertility as well as tailored therapeutic approaches to enhance fertility.

Immediately prior to the ovulatory surge of LH, the oocyte is fully grown, arrested in meiotic prophase, and enveloped by layers of cumulus cells. Within this cumulus–oocyte complex (COC), the oocyte at germinal vesicle stage secretes peptides that regulate metabolism in cumulus cells, while the cumulus cells reciprocate by providing oocytes with energy and metabolites essential for maturation and maintenance of meiotic arrest (Richani *et al.*, 2021). The COC is suspended within follicular fluid that is secreted by the multiple layers of surrounding granulosa cells (GCs), and contains serum-derived hormones and metabolites (Valckx *et al.*, 2012; Dumesic *et al.*, 2015; Pantasri *et al.*, 2015) from the vascularized theca cell layer that encircles the GCs. Thus, the ovarian follicle is a highly integrated unit in which somatic cells respond to physiological signals and are in direct communication with the oocyte.

The LH surge profoundly changes follicular cell functions, initiating a cascade of cellular signals that induce luteinization, oocyte maturation, and ovulation. GCs, which express high levels of LH-receptor (Peng *et al.*, 1991) undergo terminal differentiation to luteal cells, a process that involves a dramatic shift in metabolism (Harlow *et al.*, 1987) and the induction of steroidogenic capacity for progesterone synthesis (Plewes *et al.*, 2020; Przygrodzka *et al.*, 2021). Simultaneously, GCs release paracrine signals that act on cumulus cells to induce expansion, generating a hyaluronan-rich matrix (Park *et al.*, 2004). The oocyte responds by resuming meiosis and extruding half of the chromosomes into the first polar body in preparation for fertilization. These highly dynamic events occur rapidly and require energy generated through cellular metabolism. However, the substrate utilization and hormonal control of metabolic activity in GCs and cumulus cells under normal *in vivo* ovulatory conditions are not well understood, particularly in women.

Obesity and aging are two prevalent causes of ovarian dysfunction and female subfertility (Esencan *et al.*, 2021; Gonzalez *et al.*, 2022). Obesity in women leads to changes in the ovarian follicular environment (Andreas *et al.*, 2021) that can influence oocyte quality. For example, higher levels of insulin and triglycerides in the follicular fluid of obese women (Robker *et al.*, 2009; Valckx *et al.*, 2012, 2014) are associated with delayed embryo development (Comstock *et al.*, 2015; Leary *et al.*, 2015; Bartolacci *et al.*, 2019). However, the functional changes in ovarian somatic cells that link altered metabolite levels with poor embryo development remain to be determined. Similarly, reproductive aging alters the ovarian follicular environment (Babayev and Duncan, 2022). Compared to women less than 35 years old, follicular fluid of older women (≥40 years old) contains less glucose and more lactate (Pacella *et al.*, 2012; Dogan *et al.*, 2020). This may suggest that ovarian cells of older women have increased glycolytic activity, but this has not been directly tested. In addition, the follicular fluid of older women (>35 years old) displays more abundant lipid moieties (Cordeiro *et al.*, 2018), but whether lipid metabolism in ovarian cells is affected remains to be determined.

Mitochondria are the major sites of cellular metabolism and energy production, providing a platform for the oxidation of fuel substrates to produce ATP. The inner mitochondrial membrane is the site of the electron transport chain (ETC); a series of proteins (complex I to complex V, plus others) that maintain a proton gradient. During nutrient oxidation, reducing equivalents (NADH or $FADH_2$) generated from glycolysis, the tricarboxylic acid cycle, and β-oxidation provide electrons that pass along the mitochondrial ETC, coupled to the pumping of protons into the intermembrane space through Complexes I, III, and IV. This electrochemical gradient across the inner mitochondrial membrane drives ATP synthase (complex V) to enzymatically convert ADP to ATP. However, precisely how these metabolic processes are regulated within the ovarian follicular environment and how they might influence oocyte maturation and developmental competence has yet to be determined.

In this study, we comprehensively assessed follicular energy metabolism, specifically fatty-acid oxidation, glycolysis, and mitochondrial respiration, in ovarian GCs immediately prior to ovulation and conception. Firstly, hormonal control of GC and COC energy metabolism in response to ovulatory hCG was characterized in mouse models. We quantified the real-time oxygen consumption rate (OCR) and extracellular acidification rate (ECAR), to reveal dynamic, cell-specific changes in β-oxidation, glycolysis, and in the efficiency of mitochondrial function. Secondly, we investigated whether GC metabolism is impacted by obesity or aging, in both mouse models and in GCs from a cohort of 85 women undergoing gonadotropin-induced oocyte aspiration followed by IVF and/or ICSI. Importantly, stratification by infertility diagnosis was performed to identify any differences between cells from women deemed to have normal ovarian function compared to those diagnosed with any form of ovarian infertility. Lastly, we examined whether shifts in metabolism and/or energy production in ovarian GCs of women were associated with oocyte developmental competence. Our results show the impact of aging on normal GC metabolism and identify metabolic processes in these cells that are associated with subsequent embryonic development.

Materials and methods

Mice

All animal experiments were approved by the University of Adelaide's Animal Ethics Committee (approval no. M-2017-116 and M-2018-121) and conducted in accordance with the Australian Code of Practice for the Care and Use of Animals for Scientific Purposes. Mice were maintained in 12 h light/12h dark conditions and given water and standard rodent chow *ad libitum*. They were humanely killed by cervical dislocation immediately prior to ovarian tissue collection.

CBA F1 mice provided by Laboratory Animal Services (University of Adelaide) were used for dose optimizations and time course experiments. Mice at 3–4 weeks old were injected with PMSG (5 IU) to induce folliculogenesis, followed by an injection of hCG (5 IU) 48 h later. The ovaries were collected at 24 and 48 h after PMSG, and at 4, 8, and 12 h after hCG.

Obese or reproductively aged mice, as well as matched controls, were generated from the same colony of 'Blobby' mice (C57BL/6JSfdAnu-Alms1bbb/Apb strain; Li *et al.*, 2007) maintained as heterozygous breeding pairs, and all fed an identical standard chow diet as previously described (Wu *et al.*, 2015; Umehara *et al.*, 2022). Obese mice were homozygous (bbb/bbb) for the 'Blobby' mutation of the Alms1 gene which leads to defective basal body-ciliary function in hypothalamic neurons involved in appetite and feeding regulation (Heydet *et al.*, 2013). This mutation results in hyperphagia and profound obesity even when maintained on a standard mouse chow diet (Arsov *et al.*, 2006; Li *et al.*, 2007; Wu *et al.*, 2015; Umehara *et al.*, 2022). Before the onset of obesity, 'Blobby' females exhibit normal fertility (Arsov *et al.*, 2006; Wu *et al.*, 2015), but exhibit anovulation and reduced oocyte

developmental competence and subfertility coincident with excessive adiposity, hyperinsulinemia, and dyslipidemia (Arsov *et al.*, 2006; Wu *et al.*, 2015). Female mice were deemed obese when they weighed at least 36 g, which occurred at 4–5 months of age, and wild-type littermates were used in parallel as lean controls. Mice were considered reproductively aged at 12 months old; a model understood to be similar to women at age 40–44 years old (Flurkey *et al.*, 2007). Young/lean controls were wild-type and heterozygous females at 3 weeks or 5 months of age as indicated. Ovarian stimulation of obese, aged, and control mice was achieved by administration of PMSG and hCG, each at 5 IU/12 g of body weight.

Preparation of mouse GCs and COCs

Mice were humanely killed by cervical dislocation and ovaries were dissected and placed into αMEM media (Gibco, USA). Large pre-ovulatory follicles were punctured with a 26G needle to separately collect GCs and COCs. COCs were collected by pipette. Only intact and morphologically normal COCs were retained and any displaying poor expansion or a lack of cumulus cells (as is prevalent in COCs from mice with obesity; Wu *et al.*, 2015) were not included. GCs were simultaneously collected from the ovary by repeated puncturing into αMEM media and dispersed using hyaluronidase for 5 min with gentle pipetting. The resulting cell suspension was filtered using 70 μm cell strainers (MACS; Miltenyi Biotec Australia Pty. Ltd) to exclude any tissue fragments. GCs were then resuspended in assay media (see below) and counted using a Countess™ II FL Automated Cell Counter (Invitrogen™; USA), and the concentration adjusted to 5×10^6 cells/ml.

Assay media and compounds

All media were sterile-filtered and stored at 4°C until just before use and were used within a month.

Mitochondrial stress test assay medium: 1 mM pyruvate, 10 mM glucose, 2 mM glutamine, 15 mg/l phenol red in DMEM-based medium (glutamine was added on the day of the assay and media adjusted to pH 7.4 at 37°C).

Glycolysis assay medium: 2 mM glutamine, 15 mg/l phenol red in DMEM-based medium (glutamine was added on the day of the assay and media adjusted to pH 7.4 at 37°C).

All assay compounds/inhibitors were purchased from Sigma-Aldrich and were diluted with assay media to the indicated concentration immediately before the experiments. The optimal concentrations were determined empirically as below and in Supplementary Fig. S1.

Optimization of assay conditions

To maximize the accuracy of bioenergetic measurements, a number of factors were carefully controlled (see Schmidt *et al.*, 2021 for review), including media composition, cell density, inhibitor concentration, standardization, and normalization. Cell numbers and the concentration of mitochondrial inhibitors used in the assays were optimized using mouse GCs. The optimal number of GCs per well (150 000/well) was determined using mitochondrial stress tests and glycolysis tests conducted as recommended (Agilent Seahorse XF User Guide) using 1 μM oligomycin and 1 μM carbonyl cyanide 4-(trifluoromethoxy)phenylhydrazone (FCCP), and a combination 1 μM antimycin A and rotenone (Supplementary Fig. S1A and B). The optimal concentration of oligomycin (1.0 μM) was determined by measuring OCR and ECAR in the presence of oligomycin at concentrations of 0, 0.5, 1.0, 2.0, and 5.0 μM, and calculating the functional ratio (Supplementary Fig. S1C). To determine the optimal concentration of FCCP, maximal respiration (the ratio of OCR after FCCP to basal OCR) was measured in GCs treated with FCCP at concentrations of 0, 2.5, 5.0, and 10.0 μM; with 2.5 μM identified as the lowest effective dose (Supplementary Fig. S1D). Assay conditions for Antimycin A (1.0 μM), rotenone (1.0 μM), glucose (10 mM), and 2-deoxyglucose (2DG) (50 mM) were based on extensive literature and confirmatory pilot experiments in mouse GCs. Etomoxir was tested at concentrations of 0, 8, 40, and 100 μM; with no response in OCR observed with 8 μM and slightly excessive inhibition at 40 μM, so 30 μM was used for experiments. At 30 μM etomoxir had no detectable effect on OCR (except a modest inhibition following FCCP stimulation of maximal respiration as expected; Supplementary Fig. S2) suggesting no significant off-targets effects. Using the same assay conditions as for GCs, ≥10 COCs per well (in XFe96 Cell Culture Microplates) and ≥3 COCs per well (in XFe96 Spheroid Microplates) were within the minimum OCR and ECAR measurement ranges.

Plate coating, assay conditions, and port loading

XFe96 cell culture microplates (102416-100, Agilent Technologies) were used for GCs. COCs in the time course were cultured in XFe96 cell culture microplates and COCs in the obesity experiments were cultured in XFe96 Spheroid Microplates (102905-100, Agilent Technologies). The microplates were coated with fibronectin (Sigma-Aldrich F1141) dissolved in double-distilled water according to the manufacturer's instructions, used at 15 μg/cm^2, and incubated in a humidified 37°C non-CO_2 incubator for at least 1 h. The plate was washed twice with the appropriate assay medium before the experiment.

Substrate (long chain fatty acid) oxidative stress tests were performed with the following compounds: (Port A) Etomoxir (30 μM) or, for the control group, assay medium; (Port B) oligomycin (1 μM); (Port C) FCCP (2.5 μM); and (Port D) a combination of antimycin A and rotenone (1 μM each). Each compound was dissolved in mitochondria stress test assay medium.

Glycolysis assays were performed with the following compounds: (Port B) glucose (10 mM); (Port C) oligomycin (1 μM); and (Port D) 2DG (50 mM). Each compound was dissolved in glycolysis assay medium.

Mitochondria stress test assays were performed with the following compounds: (Port A) mitochondrial stress test medium; (Port B) oligomycin (1 μM); (Port C) FCCP (2.5 μM); and (Port D) a combination of antimycin A (1 μM) and rotenone (1 μM). Each inhibitor was dissolved in the mitochondria stress test assay medium.

ATP production rate assays were performed with the following compounds: (Port B) oligomycin (1 μM); and (Port C) a combination of antimycin A and rotenone (1 μM each). Each compound was dissolved in mitochondria stress test assay medium.

Seahorse XF analyzer (XFe96) assay

OCR and ECAR were measured using a Seahorse XF analyzer (XFe96; Agilent Technology). The day before the experiment, the XFe96 machine was equilibrated to 37°C and the sensor cartridge was hydrated in Seahorse XF Calibrant at 37°C overnight. The day of the experiment, the assay medium (150 μl/well) was loaded to the assay plate and the compounds loaded into the injection ports of the sensor cartridge. The volume of each well of the assay plate was prepared to a final volume of 180 μl, and the injection ports were prepared in order of A: 20 μl, B: 22 μl, C: 25 μl, D: 27 μl. The sensor cartridge was loaded into the machine and calibrated. Meanwhile, the cells were prepared (see above) and 30 μl of the cell solution (5×10^6 cells/ml) was added to the 150 μl of assay media in each well to make a final well volume of 180 μl

and the plate centrifuged for 1 min at 1500*g* to plate cells. This cell density (15×10^4 live cells/well) was optimized at the outset of these experiments (see above and Supplementary Fig. S1). Intact COCs were added to the center of each well (10 COCs per well for XFe96 cell culture microplates or 3 COCs per well for XFe96 Spheroid Microplates). To avoid positional variation, the corner wells of the plates were blanks containing media but no cells, and replicate experiments varied the positions of the treatment groups on the plate. The cells were incubated for 15 min at 37°C prior to starting the assay. The assay plate was loaded into the machine, and cells were measured in cycles of 3 min of mixing and 3 min of measurement. The time from tissue dissection to plate loading into the Seahorse analyzer was kept within 2 h to avoid negative effects on cell viability and alterations to metabolism.

Patient background

The use of human GCs in this study was approved by the St Andrew's Hospital HREC (STAND Project No. 93) and the University of Adelaide HREC (No. H-2021-085). Human GCs were collected as part of routine oocyte aspiration from women attending Genea Fertility SA (Adelaide, Australia) and were donated to research instead of being discarded. There were no specific inclusion or exclusion criteria and on days when two to five patients were scheduled for egg retrieval, they were sequentially enrolled. The 85 patients were undergoing either gonadotrophin-releasing hormone antagonist- or agonist-stimulated IVF/ICSI cycles. FSH doses were based on the standard clinic protocols. FSH products used were Gonal-F (Merck Group, Darmstadt, Germany), Puregon (Merck Sharp & Dohme BV, Haarlem, The Netherlands), or Menopur (Ferring Pharmaceuticals, Saint-Prex, Switzerland), ranging between 150 IU and 400 IU. Upon identification of three follicles exceeding 17 mm in width via transvaginal ultrasonography, patients received an HCG trigger shot (5000–10 000 IU) within a 24- to 48-h window, followed by transvaginal oocyte retrieval 36- to 38-h post-HCG. During this procedure, follicular contents were aspirated into oocyte collection tubes (Vitrolife), from which COCs were isolated and used for the patient's fertility treatment. The remaining follicular aspirate from each patient was then utilized for GC isolation.

Human GC isolation

Follicular aspirates, which contained only GCs and not cumulus cells, were gently centrifuged in 50 ml tubes at 400 *g* for 3 min. The supernatant was discarded, and cells were treated with hyaluronidase (10 IU in 10 µl) for 5 min to prevent aggregation. Red blood cell lysis buffer (NH_4Cl: 150 mM, $NaHCO_3$: 10 mM, EDTA: 1 mM) was added to 50 ml and the tube was gently shaken for 10 min to resuspend the cell pellet. The solution was filtered with 70 µm cell strainers to remove any blood clots or cell clumps. The filtered cell solution was centrifuged at 400*g* for 3 min and the supernatant was completely aspirated. Cells were resuspended in assay medium (see above), counted, and adjusted to a concentration of 5×10^6 cells/ml. 30 µl of the cell solution was added to each well of a prepared assay plate (see above) and the plate was centrifuged at 400*g* for 1 min and incubated in a humidified 37°C non-CO_2 incubator for 15 min. The plate was then loaded into the Seahorse Bioanalyzer.

Human *in vitro* fertilization, embryo culture, and scoring

Independent from this research, COCs recovered from follicular aspirates were placed in G-MOPS^{TM} PLUS (Vitrolife, Frölunda, Sweden), then in G-IVF^{TM} PLUS (Vitrolife) until insemination or denudation. Oocyte fertilization methods included standard IVF or ICSI, determined by individual treatment plans. For conventional IVF, COCs (up to five) were co-incubated with sperm (~160 000/ml) for 2 h in G-IVF^{TM} PLUS. Post-insemination, oocytes were transferred to G1 PLUS (Vitrolife). For ICSI procedures, COC denudation involved 75 IU/ml Hylase® (CP Pharmaceuticals, Wrexham, UK) combined with fine bore pipetting. Denuded oocytes awaited injection in G1 PLUS. Post-injection, groups of four oocytes or less were situated in 50 µl G1 PLUS droplets, overlaid with Ovoil (Vitrolife, Göteborg, Sweden).

Day-1 post-fertilization, embryos were cultured in groups of up to four, until Day 5. On Day 3, embryo assessment was conducted with on-time embryos identified as having seven or more blastomeres at 68 h after insemination. These embryos were transferred into G2 PLUS medium (Vitrolife). All culture settings were pre-equilibrated, with oocytes and embryos cultured in BT37 Mark II benchtop incubators (PLANER, Middlesex, UK) in an atmosphere of 6% CO_2, 5% O_2, and 89% N_2. On Day 5, embryos were deemed good quality blastocysts if they were scored as grade 2 or over for expansion with scores of either A or B for both trophectoderm and inner cell mass (Gardner, 1999). Oocyte developmental competence and embryo assessments were obtained from patient records to perform correlative analyses with GC metabolism at time of egg retrieval.

Statistical analysis

OCR and ECAR data were processed using Wave software (Agilent Technologies) and outputs generated using the appropriate recommended calculations and no additional corrections to the data. Energy maps were created using Wave software (Agilent). ATP Production Rates were inferred from changes in the OCR and determined using XF Real-time ATP Rate Assay Report Generator (Agilent) and the following explicit reaction schemes and assumptions: (i) mitoATP production rate (Basal): [(Last OCR rate measurement before first injection − Minimum OCR rate measurement after oligomycin but before Rot/AA injection) × 2 × (oxidative phosphorylation per oxygen atom consumed, P/O ratio)]; (ii) glycoATP Production Rate (Basal): Last glycol OCR measurement before first injection; (iii) Total ATP production rate (basal): (mitoATP production rate)+(glycoATP production rate).

In mouse GC assays, each datapoint is an average of readings from ≥4 wells containing cells pooled from three to six mice. In the COC assays, each datapoint is the mean of ≥3 wells of COCs collected from multiple mice. Data from COCs in the time course were normalized to cell number. COCs in the obesity experiments were standardized to three COCs per well. In human GC assays, each datapoint is an average of readings from ≥4 wells containing cells from a single patient.

Power analysis based on preliminary assays in cells from a small number of patients prior to the start of the main study and estimation of an enrolment ratio of 1:3 (normal ovarian function: ovarian infertility) showed that a sample size of 21 (normal ovarian function) and 64 (ovarian infertility) provides >95% power (alpha 0.05).

Statistical analysis was performed with Graph Pad Prism 9 and R software. Unpaired two-tailed *t*-tests were used for comparisons between two groups, and one-way ANOVA with Tukey's multiple comparisons was used for comparisons of more than two groups. Analysis of data from human cells was performed using Spearman r correlation to account for non-parametric associations. For all statistical tests, a value of $P < 0.05$ was deemed to be statistically significant. *P*-values are indicated by asterisks in the legends. *$P < 0.05$; **$P < 0.01$; ***$P < 0.001$; ****$P < 0.0001$.

Results

Murine GCs and COCs display distinct metabolic profiles during ovulation

GCs and COCs from mouse ovaries at 24 and 48 h after PMSG (FSH analog), and at 4, 8, and 12 h after an ovulatory dose of hCG were analyzed using extracellular flux analysis of fatty acid oxidation (FAO), glycolysis, and mitochondrial respiration. For FAO assays, OCR was measured in the presence versus absence of etomoxir, which inhibits the transport of fatty acid-CoA (FA-CoA) into the mitochondria (see Fig. 1A). The differential in values provides a measure of OCR that is due to β-oxidation of long-chain fatty acids (Supplementary Fig. S2). In GC, no changes in OCR were observed between 24 and 48 h following PMSG stimulation or up to 8 h after hCG (Fig. 1B). However, fatty acid metabolism (i.e. etomoxir-sensitive respiration) was significantly increased just before ovulation, with a 3-fold induction at 12 h after hCG compared to levels immediately before hCG, at PMSG 48 h (Fig. 1B). Maximal FAO function, defined as the capacity for FAO following mitochondrial uncoupling, was increased within 8 h following hCG (Fig. 1C). Because FAO analysis requires twice as many cells as the other metabolic assays, COCs could not be assessed in parallel. However, these data demonstrate that ovulatory hCG induces long-chain fatty acid metabolism in GCs near the time of ovulation, and complements previous observations demonstrating an increase in fatty acid uptake and FAO metabolism in COCs that is concurrent with LH-induced oocyte maturation and essential for subsequent preimplantation embryo development (Dunning *et al.*, 2010; Aardema *et al.*, 2011; Van Hoeck *et al.*, 2013; Paczkowski *et al.*, 2014; Sanchez-Lazo *et al.*, 2014).

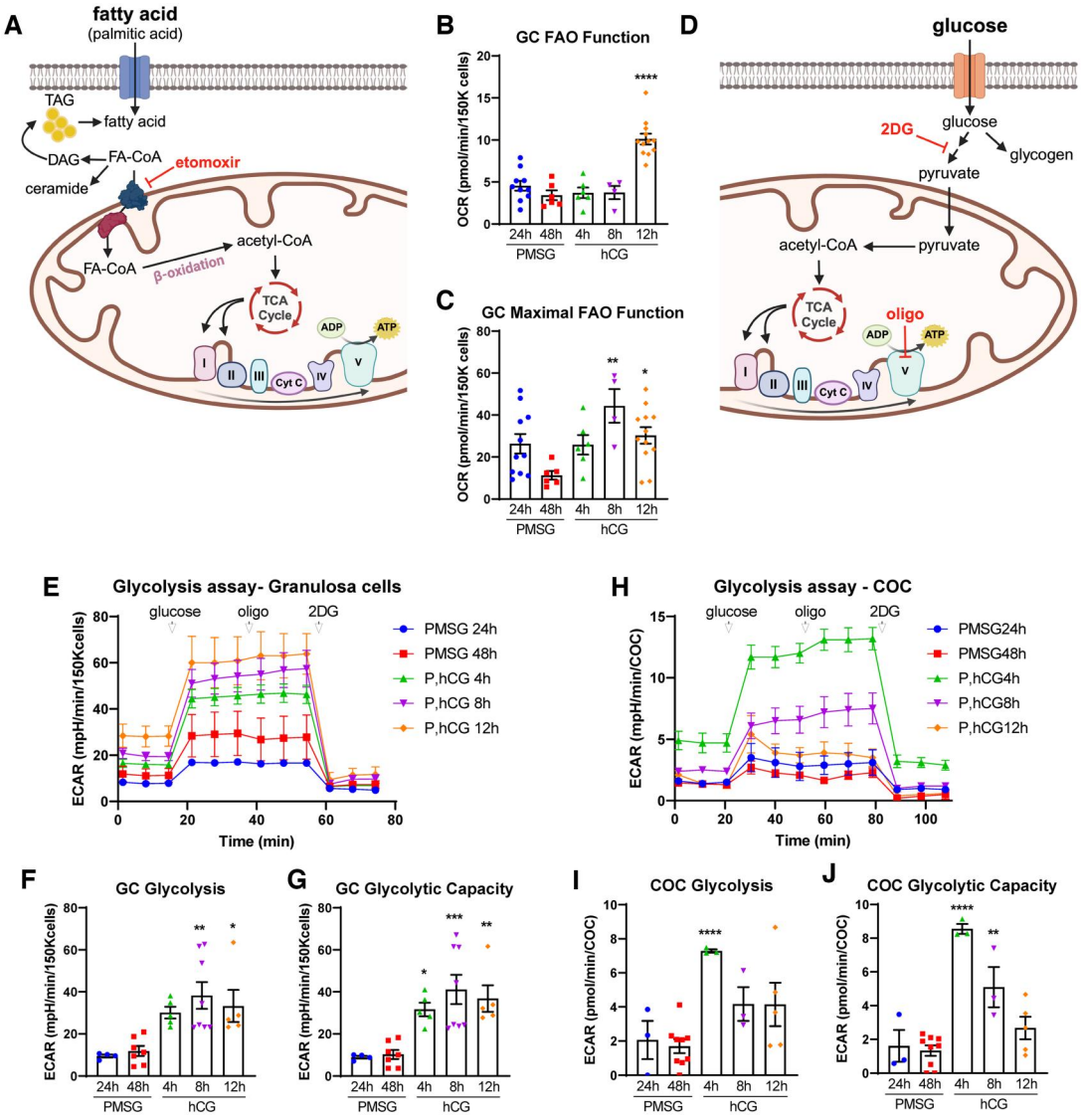

Figure 1. Fatty acid oxidation and glycolysis in mouse granulosa cells (GCs) and cumulus–oocyte complexes (COCs) in response to ovulatory hormones. (**A**) Schematic representation of fatty acid oxidation (FAO) and inhibitory action of etomoxir. (**B**) FAO function and (**C**) maximal FAO function were quantified in mouse GCs (150K cells/well) collected at 24 and 48 h after PMSG (P), and 4, 8, and 12 h after hCG. N = 4–12 pools of cells from different mice collected at each timepoint. (**D**) Schematic representation of glycolysis and inhibitory actions of oligomycin (oligo) and 2-deoxyglucose (2DG). (**E**) Extracellular acidification rate (ECAR) millipH/min (mpH/min) was measured in GCs collected from mice at 24 and 48 h after PMSG, and at 4, 8, and 12 h after hCG to determine glycolytic functions: glycolysis (**F**) and glycolytic capacity (**G**). N = 4–8 pools of cells from multiple mice collected at each timepoint. (**H–J**) ECAR was measured in COCs from the same mice, in parallel to the GCs. N = 3–9 pools of COCs from multiple mice collected at each timepoint. Data shown as mean ± SEM. Statistical analysis by one-way ANOVA with comparison to cells collected at PMSG 48 h. *$P < 0.05$; **$P < 0.01$; ***$P < 0.001$; ****$P < 0.0001$ compared to PMSG 48 h.

To analyze glycolysis, we measured the ECAR (milli-pH/minute (mpH/min)), an established and widely used indicator of glycolysis. GCs and COCs were collected from mice at 24 and 48 h after PMSG, and at 4, 8, and 12 h after an ovulatory dose of hCG. Glycolytic function assays (see Fig. 1D) provide glucose as an energy substrate and then sequentially inhibit Complex V (using oligomycin) and glucose metabolism (using 2DG) to isolate distinct aspects of glycolytic metabolism. In GCs, glycolysis (i.e. glucose-stimulated ECAR) did not change between 24 and 48 h after PMSG stimulation, but was significantly increased following hCG, peaking at 8 h (Fig. 1E and F). Glycolytic capacity showed an identical pattern (Fig. 1E and G), demonstrating that GCs operate at their maximum level of glycolysis. As such, glycolytic reserve was exceedingly low or undetectable at all timepoints (data not shown). In COCs, glycolytic metabolism was regulated differently compared to GCs. Glycolysis and glycolytic capacity peaked at 4 h after hCG (Fig. 2H–J), which is earlier than that observed in GCs, before both declined. Similar to GCs, glycolytic reserve in COCs was below detection levels (data not shown). These results indicate that GCs continuously increase cellular respiration in response to ovulatory hCG, while COCs exhibit a burst of respiration at 4 h, followed by a decline in glycolytic metabolism.

Hormonal regulation of mitochondrial respiration in mouse GCs and COCs was examined by measuring the OCR in response to specific inhibitors of ETC components (see Fig. 2A), known as the 'mitochondrial stress test'. In GCs, most metabolic measures were lowest immediately prior to the LH surge (i.e. at PMSG 48 h) and maximal at the time of ovulation (i.e. P, hCG 12 h). Specifically, basal respiration (OCR), inferred ATP production (oligomycin-sensitive OCR), maximal respiration (FCCP-sensitive OCR), and spare respiratory capacity (actinomycin A-/rotenone-sensitive OCR) were each increased at 12 h after hCG compared with all earlier timepoints (Fig. 2B–F). Mitochondrial proton leak (oligomycin-independent OCR) was also maximal at 12-h post-hCG (Fig. 2G), while coupling efficiency (ATP production as a function of basal respiration) remained relatively constant at all timepoints (Fig. 2H). Together, these data demonstrate that aerobic mitochondrial function (OxPhos) in GCs peaks at the time of ovulation, while anaerobic glycolytic function increases more rapidly, peaks earlier at 8-h post-hCG, and remains high at the 12 h timepoint (Fig. 1E–G). COCs exhibited a dramatically different mitochondrial metabolic pattern (Fig. 2I–O): basal respiration, inferred ATP production, and maximal respiration peaked at 4 h after hCG, after which OCR gradually returned to similar levels as before the administration of hCG (Fig. 2I–L). Furthermore, COCs exhibited modest spare respiratory capacity (Fig. 2M) when compared to the high levels observed in GCs (Fig. 2F). Proton leak was also only transiently increased 4 h after hCG in COCs (Fig. 2N); while there was a concurrent decrease in coupling efficiency (Fig. 2O). Thus, in COCs, glycolysis and mitochondrial metabolism are regulated synchronously, with a dramatic but transient peak specifically at 4-h post-hCG. Importantly, these observations demonstrate that cumulus cell metabolism near the time of ovulation is not indicative of maximal metabolic capacity.

ATP Production Rates, derived from changes in the OCR, were used to directly compare OxPhos (aerobic mitochondrial metabolism) and glycolysis (anaerobic metabolism) in energy maps which further demonstrated that GCs and COCs exhibit distinct kinetics in response to hCG (Fig. 3A and D). GCs increase both forms of metabolism in response to hCG and then further upregulate OxPhos by 12-h post-hCG (Fig. 3A). In contrast, COCs increase anaerobic glycolysis within 4-h post-hCG and by 12-h post-hCG have returned to baseline levels of metabolism similar to that in immature COCs prior to ovulatory hCG (Fig. 3D). These estimated ATP production assays revealed additional interesting differences between GCs and COCs. In GCs, total ATP production showed no statistically significant increase until 8 h after hCG (Fig. 3B). COCs again displayed a different profile, with ATP production much lower overall, and rapidly increasing at 4 h after hCG before decreasing toward the levels seen prior to hCG (Fig. 3E). GCs had a higher rate of ATP production from OxPhos that did not significantly change with hormonal stimulation (Fig. 3C), while COCs had a higher rate of ATP production from glycolysis that also stayed relatively constant across the ovulatory cycle (Fig. 3F).

Together, these data establish fundamental baseline metabolic profiles for GCs and COCs in response to ovulatory hormones. Importantly, these assays were conducted using the standard base medias (i.e. DMEM with only pyruvate, glucose, and glutamine) to directly compare cell-intrinsic metabolic changes in response to hCG. The *in vivo* physical and nutritional microenvironment of the ovulating follicle, specifically increased vascular permeability and serum influx, would provide additional regulation. However, the direct comparison of the two cell types under identical conditions demonstrates that COCs more quickly upregulate ATP production in response to hCG but exhibit relatively lower levels of mitochondrial respiration than GCs.

Obesity and aging disrupt the metabolic profile of mouse GCs at ovulation

Toward investigating whether GC mitochondrial function, glycolytic function, and ATP production are impacted by obesity or aging, we first demonstrated that our methods are sensitive to detect changes in the ETC, using a targeted model of Complex I inhibition. Specifically, female mice were fed rotenone, an inhibitor of mitochondrial Complex 1 (see Fig. 2A), for 2 weeks before GCs were isolated 8-h post-hCG. Marked inhibition of mitochondrial function, glycolysis, and ATP production were detected (Supplementary Fig. S3), confirming the sensitivity of the assays to detect metabolic changes in isolated GCs.

To determine the effects of obesity on energy metabolism in GCs, we used a hyperphagic mouse model. Following significant weight gain and the onset of hyperinsulinemia and dyslipidemia, the obese female mice exhibit anovulation, reduced oocyte developmental competence, and subfertility (Arsov *et al.*, 2006; Wu *et al.*, 2015; Umehara *et al.*, 2022), similar to infertility phenotypes observed in obese women (Gonzalez *et al.*, 2022). Metabolic profiles were compared in cells derived from either lean or obese mice at 10-h post-hCG (Fig. 4A–C). Obesity significantly reduced the key mitochondrial parameters of basal respiration, inferred ATP production, and maximal respiration (Fig. 4A and D–G; Supplementary Fig. S4A and B). Conversely, glycolytic function and FAO in GCs from obese mice were indistinguishable from that in lean controls (Fig. 4B and C; Supplementary Fig. S4C–G). The estimated amount of ATP produced by OxPhos and glycolysis was not different nor significantly altered by obesity ($P = 0.066$); however, there was a significant interaction between the two variables with obesity causing a significant reduction in OxPhos ($P = 0.04$) but not glycolysis (Fig. 4H). ATP production rate (the percentage produced by each form of metabolism) showed a greater proportion resulting from OxPhos (Fig. 4I), but this ratio was not significantly altered by obesity ($P = 0.063$). Interestingly, the metabolic profile of COCs was unchanged by obesity (Supplementary Fig. S5A–C). No statistically significant differences were found between COCs obtained from obese or lean mice

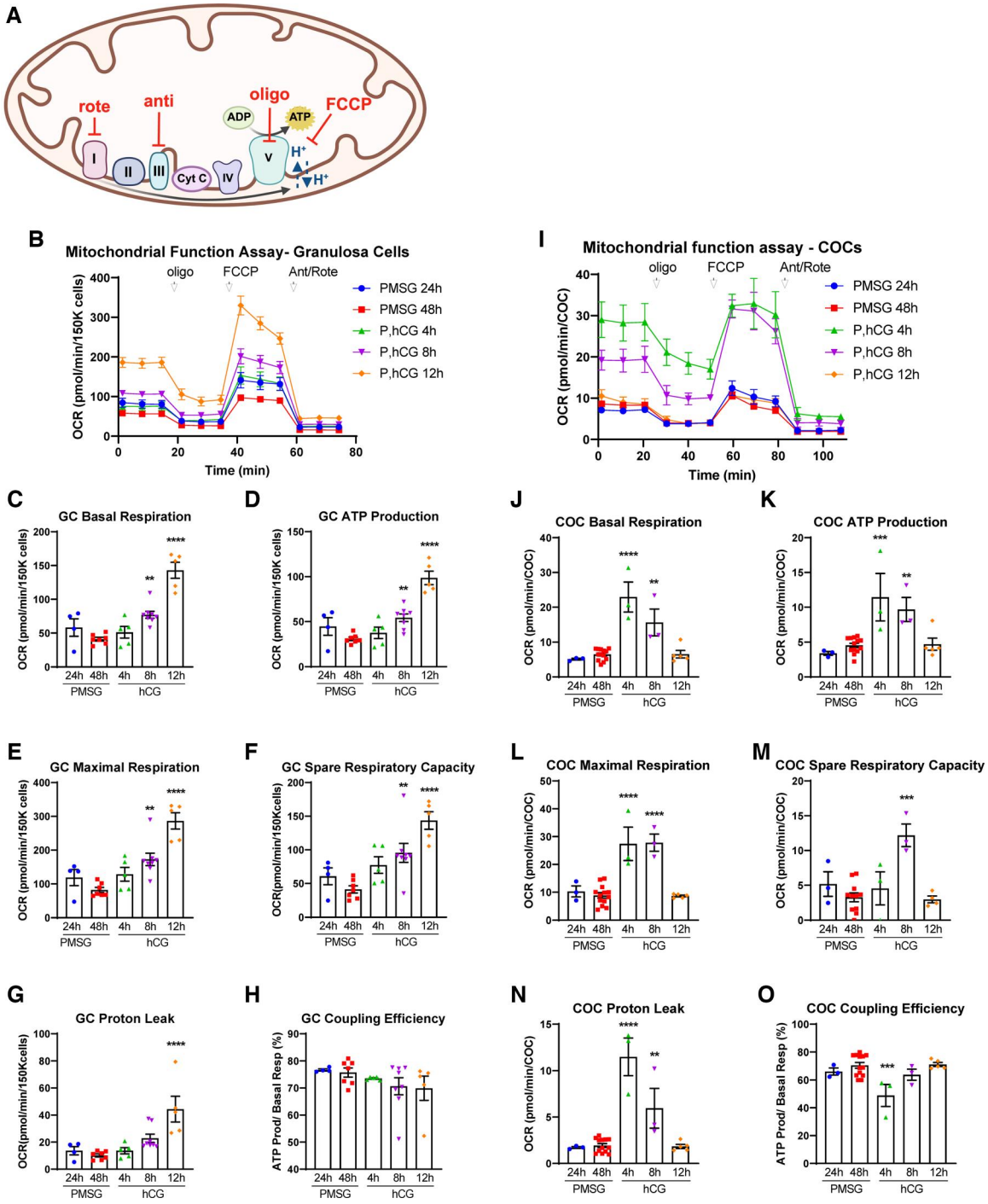

Figure 2. Mitochondrial metabolism in mouse granulosa cells (GCs) and cumulus–oocyte complexes (COCs) in response to ovulatory hormones. (**A**) Schematic representation of mitochondrial metabolism and inhibitory actions of rotenone (rote), antimycin A (anti), oligomycin (oligo), and Carbonyl cyanide 4-(trifluoromethoxy)phenylhydrazone (FCCP). (**B**) Oxygen consumption rate (OCR) (pmol/min) was measured in GCs (150K cells/well) collected from mice at 24 and 48 h after PMSG (P), and at 4, 8, and 12 h after hCG. Basal respiration (**C**); ATP production inferred from OCR (**D**); maximal respiration (**E**); spare respiratory capacity (**F**), protein leak (**G**), and coupling efficiency (**H**) were determined. N = 4–8 pools of cells from multiple mice collected at each timepoint. (**I–O**) OCR was measured in mouse COCs in parallel to the GCs. N = 3–13 pools of COCs from multiple mice collected at each timepoint. Data shown as mean ± SEM. Statistical analysis by one-way ANOVA with comparison to cells collected at PMSG 48 h. $^{**}P < 0.01$; $^{***}P < 0.001$; $^{****}P < 0.0001$ compared to PMSG 48 h.

in any parameter of mitochondrial function (Supplementary Fig. S5D–H), glycolysis (Supplementary Fig. S5I and J), or fatty acid metabolism (Supplementary Fig. S5K and L). These findings demonstrate that obesity impacts mitochondrial function in GCs during ovulation and oocyte maturation but does not affect glycolysis or FAO in these cells.

To determine the effects of aging on the metabolism of mouse GCs, we compared the metabolic profiles of cells from 3-week-old mice (pre-pubertal), 5-month-old mice (adult, peak fertility), and 1-year-old mice (middle-age, low fertility) which are comparable to 40–44 years old in women (Flurkey *et al.*, 2007). COCs could not be analyzed because of the very low numbers found in

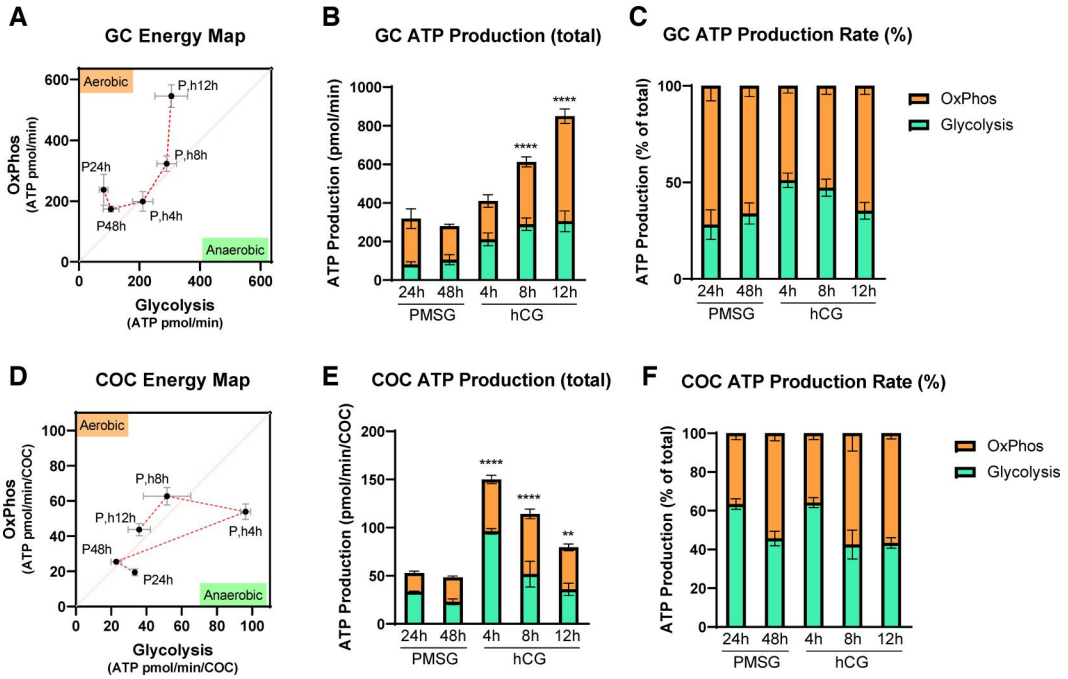

Figure 3. ATP production via oxidative phosphorylation (OxPhos) and glycolysis in mouse granulosa cells (GCs) and cumulus–oocyte complexes (COCs) in response to ovulatory hormones. O_2 consumption (OCR) and extracellular acidification (ECAR) in GCs and COCs collected from mice at 24 and 48 h after PMSG (P), and 4, 8, and 12 h after hCG (h) are used to generate energy maps and to infer ATP production rates. Energy maps in GCs (**A**) and COCs (**D**). The sequence of the ovulatory time course is indicated by the red dotted lines. Quantification of inferred ATP production in GCs (**B**) and in COCs (**E**). Percentage of OxPhos versus glycolysis in ATP production in GCs (**C**) and in COCs (**F**). N = 4–8 pools of GCs from multiple mice collected at each timepoint. N = 3–10 pools of COCs collected from the same mice. Data shown as mean ± SEM. Statistical analysis (B, C, E, F) by one-way ANOVA with comparison to cells collected at PMSG 48 h. $^{**}P < 0.01$; $^{****}P < 0.0001$ compared to PMSG 48 h.

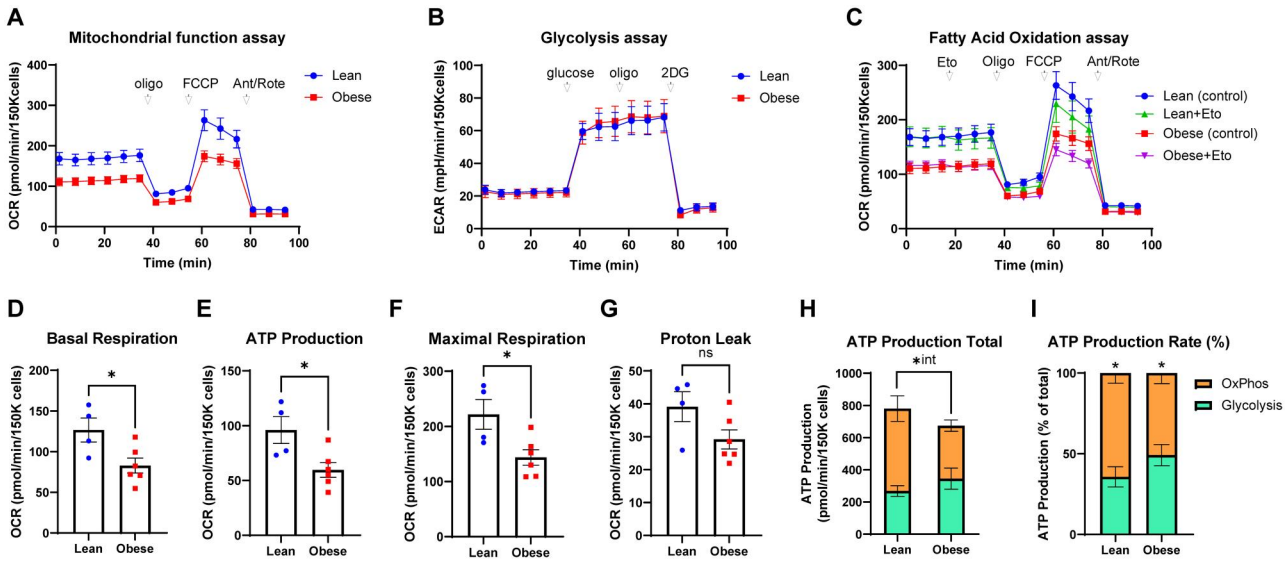

Figure 4. Metabolic effects of obesity on mouse granulosa cells (GCs). Mitochondrial respiration, glycolysis, fatty acid oxidation (FAO), and ATP production were measured in GCs derived from lean or obese mice at 8-h post-hCG. (**A**) Mitochondrial function assay; (**B**) glycolytic function assay; (**C**) FAO function assay; (**D**) basal respiration; (**E**) ATP production inferred from oxygen consumption rate; (**F**) maximal respiration; (**G**) proton leak; (**H**) total ATP production; and (**I**) ATP production rate from OxPhos versus glycolysis. N = 4 pools of granulosa cells from obese mice and N = 6 pools of cells from obese mice. Data shown as mean ± SEM. Statistical analysis by unpaired two-tailed *t*-test: ns $P > 0.05$, $^{*}P < 0.05$, *int = significant interaction between obesity and OxPhos.

the ovaries of aged mice. Additionally, obese 5-month-old and obese 1-year-old mice were included for direct comparison of effects caused by aging and obesity. Aging, between 5 months and 1 year of age, led to significant reductions in most measures of mitochondrial function (Fig. 5A–G). These reductions were strikingly exacerbated by obesity, with cells from the 1-year-old obese mice exhibiting very low to negligible metabolic activity (Fig. 5A–F, orange symbols). Glycolytic function was also significantly reduced in aged mice, between 5 months and 1 year of age (Fig. 5H–J). As with mitochondrial respiration, obesity significantly exacerbated the glycolytic changes, with extremely low glycolytic metabolism observed in 1-year-old mice that were also obese (Fig. 5H–J, orange symbols). Thus, aging caused metabolic alterations similar to the mitochondrial toxicant rotenone (see

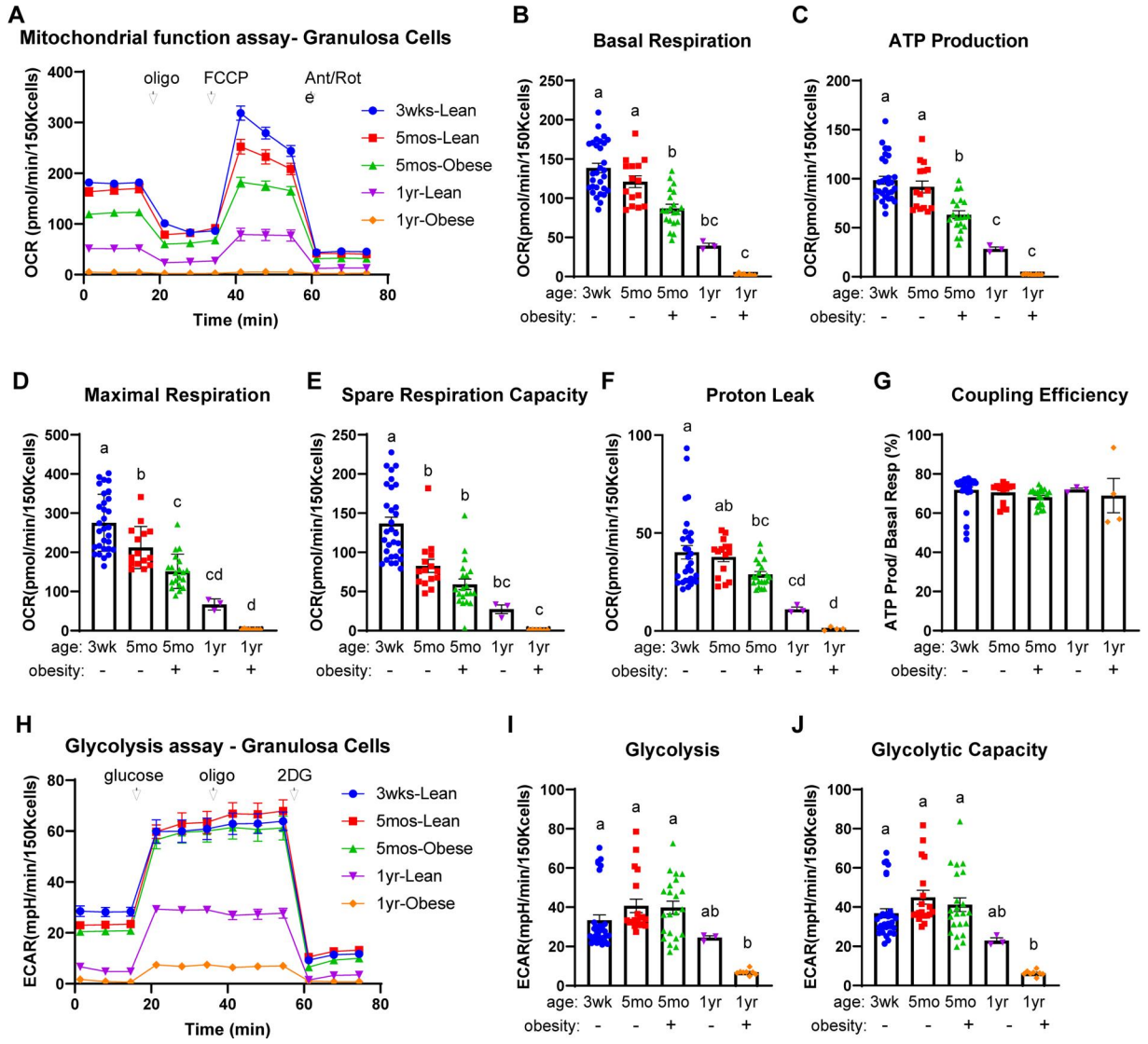

Figure 5. The effects of age and obesity on mitochondrial and glycolytic function in mouse granulosa cells (GCs). GCs were collected from mice that were 3 weeks old, 5 months old (lean or obese littermates), or 1 year old (lean or obese littermates) at 12-h post-hCG. Mitochondrial function assay (**A**); basal respiration (**B**); ATP production inferred from oxygen consumption rates (OCR) (**C**); maximal respiration (**D**); spare respiration capacity (**E**); proton leak (**F**); and coupling efficiency (**G**) in GCs from the indicated type of mice. N = 30 (3 weeks lean); N = 15 (5 months-lean); N = 20 (5 months-obese); N = 3 (1 year-lean); N = 8 (1 year-obese) pools of GCs. Glycolytic function assay (**H**); glycolysis (**I**); and glycolytic capacity (**J**) in GCs from the indicated types of mice. N = 31 (3 weeks lean); N = 19 (5 months-lean); N = 22 (5 months-obese); N = 3 (1 year-lean); N = 8 (1 year-obese) pools of GCs. Data shown as mean ± SEM. Statistical analysis by one-way ANOVA. Different letters indicate a statistically significant difference ($P < 0.05$) between groups.

Supplementary Fig. S3), and the combination of reproductive aging and obesity led to the most severe reductions in the metabolism of mouse GCs.

Aging reduces mitochondrial function in human GCs

To determine if similar metabolic sensitivity to aging and obesity occurs in cells of women, we examined GCs collected from a cohort of patients attending a local fertility clinic (Genea Fertility SA; Adelaide, Australia). A total of 85 patients (mean age 35.5 ± 4.6 years (range 26–44); mean BMI 27.4 ± 4.6 (range 17.0–53.2)) who had received gonadotropin induction and were undergoing IVF and/or ICSI were included in the study (Supplementary Table S1). Patients were further classified into 'Normal Ovarian Function' (n = 21) or 'Ovarian Infertility' (n = 64) according to the presence or absence of reduced ovarian function (Supplementary Table S1). The Normal Ovarian Function group included patients with tubal or male factor infertility, while the Ovarian Infertility group included patients with endometriosis, PCOS, or unexplained infertility (Supplementary Table S1). FAO, glycolysis, and mitochondrial respiration were measured in the GCs of each woman immediately after follicular aspiration and removal of the COCs.

Correlation analysis investigated the presence of relationships between the GC metabolic measures with age or BMI. Analysis of the entire cohort (Supplementary Table S2 and Fig. S6A–D) showed that aging was associated with decreased mitochondrial respiration and inferred ATP production, but aging was not correlated with any changes in glycolytic metabolism or long-chain FAO. In contrast, increasing BMI was associated with decreased FAO function and reduced proton leak in conjunction with increased efficiency of ATP production (Supplementary Table S2). These findings indicate that aging can disrupt mitochondrial function in human GCs, while increased adiposity (i.e. higher BMI) may impede FAO. Metabolic profiles of GCs from the Normal Ovarian Function group showed a range of OCR

responses that did not segregate from those of the rest of the cohort (Supplementary Fig. S6E and F). However, when the cohort was stratified by ovarian infertility diagnosis, distinct influences of age and BMI on GC metabolism emerged (Table 1; Supplementary Table S2). The efficiency of mitochondrial ATP production (coupling efficiency) was significantly disrupted by age, regardless of ovarian function diagnosis (Table 1). However, in patients with ovarian dysfunction, multiple additional aspects of mitochondrial respiration were negatively correlated with age (Table 1). Specifically, maximal respiration, spare respiratory capacity, and the proportion of ATP generated by mitochondria were all significantly reduced with age (Table 1). The correlation between increasing BMI and decreasing proton leak was also only observed in the ovarian infertility group (Table 1; Supplementary Table S2). These negative associations were not apparent in the GCs of the Normal Ovarian Function group (Table 1). No significant correlations were found between age or BMI and glycolytic or FAO functions in the two groups stratified by ovarian function (Supplementary Table S2). These results suggest that age-associated reductions in mitochondrial function in ovarian GCs contribute to female infertility.

Granulosa metabolic measures correlate with fertilization and embryonic development

Number of oocytes aspirated and fertilization outcomes, recorded as standard of care, were obtained for each patient. As expected, the number of eggs retrieved was decreased with age (Supplementary Table S3; Broekmans *et al.*, 2009), but otherwise, there were no significant effects of age or BMI on embryo outcomes (fertilization rate, on-time Day 3 development, or blastocyst formation rates) in either the Normal Ovarian Function group or the Ovarian Infertility group (Supplementary Table S3). The number of eggs retrieved was positively correlated with spare respiratory capacity (Supplementary Table S4), suggesting that higher mitochondrial reserve capacity is a beneficial parameter for follicle growth.

To investigate how GC energy metabolism affects oocyte developmental competence, we investigated the relationships between FAO, glycolysis, mitochondrial respiration in GC, and subsequent embryonic development in each patient. Surprisingly, higher GC metabolism (of any type) was associated with reduced fertilization rates (Supplementary Table S4). This association could be visualized graphically as clearly higher OCR and ECAR profiles in GCs of women with the lowest fertilization rates (Supplementary Fig. S6G and H). When the cohort was stratified to examine women with Normal Ovarian Function compared to Ovarian Infertility, it revealed that this negative correlation between energy metabolism in GCs and fertilization rate occurred only in women with Ovarian Infertility (Table 2). Again, this relationship was observed for each type of cellular respiration (Table 2), specifically FAO function and glycolytic function (glycolysis and glycolytic capacity). Multiple aspects of mitochondrial respiration were also inversely correlated with the rate of fertilization; namely, basal respiration, inferred ATP production, proton leak, and total estimated ATP production (Table 2). Notably, these metabolic markers are distinctly different from those impacted by age (maximal respiration, spare capacity, and coupling efficiency; Table 1). These results indicate that excessive metabolic rates in GCs of some women with ovarian infertility may be detrimental to oocyte quality.

Metabolic measures associated with successful embryo outcomes were also identified. In women with normal ovarian function, coupling efficiency (the efficiency of ATP production by mitochondria) was positively associated with fertilization rate (Table 2). Likewise, glycolytic reserve in GCs was positively associated with on-time embryo development at Day 3 (Table 2). In patients with ovarian infertility, where fertilization resulted in embryo development, the balance of ATP production was positively correlated with blastocyst formation (Table 2). Specifically, patients with higher mitochondrial function in GCs relative to the glycolytic system had better blastocyst development rates (Table 2), further indicating that improved efficiency of mitochondrial ATP production in GCs is associated with better embryonic development. In sum, these analyses demonstrate that metabolic function in GCs at the time of egg retrieval is associated with distinct aspects of oocyte developmental competence.

Discussion

This study demonstrates the dynamic regulation of multiple energy metabolism pathways in ovarian GCs in response to the ovulatory LH surge. In addition, we show that aging in women specifically reduces mitochondrial respiration in GCs, more so than fatty acid metabolism or glycolysis. Finally, we identify distinct metabolic measures in GCs that positively, and negatively, correlate with fertilization rates and on-time embryo development following IVF/ICSI. These results indicate that GC metabolism near the time of ovulation influences the health and competency of maturing oocytes.

We compared cells from women deemed to have normal ovarian function with those from women with documented ovarian dysfunction, to better understand normal GC metabolism and to

Table 1. Correlation of age and BMI with energy metabolism in patients with normal or abnormal ovarian function.

	Normal ovarian function (n = 21)		Ovarian infertility (n = 64)	
Metabolic parameters	**Age**	**BMI**	**Age**	**BMI**
Mitochondrial function				
Basal respiration	0.152	0.073	−0.164	−0.182
ATP production	−0.010	0.082	−0.217	−0.126
Maximal respiration	−0.079	0.099	**−0.344****	−0.042
Spare respiratory capacity	−0.153	0.105	**−0.377****	0.039
Proton leak	0.348	0.040	−0.065	**−0.261***
Coupling efficiency (%)	**−0.452***	0.278	**−0.336****	0.239
ATP production rate				
Total ATP production	0.318	0.029	−0.132	−0.239
Mitochondrial ATP (%)	−0.168	−0.231	**−0.253***	−0.005
Glycolytic ATP (%)	0.168	0.231	**0.253***	0.005

Bold numbers indicate significant correlations.
* $P < 0.05$. ** $P < 0.01$.

Table 2. Correlation between energy metabolism and embryonic development in patients with normal or abnormal ovarian function.

	Normal ovarian function (n = 21)			Ovarian infertility (n = 64)		
Metabolic parameters	Fertilization rate (%)	On time Day 3 (%)	Blastocyst (%)	Fertilization rate (%)	On time Day 3 (%)	Blastocyst (%)
FAO function						
FAO function	0.122	0.105	0.064	**−0.317***	−0.056	−0.149
Maximal FAO function	0.031	0.109	0.262	−0.171	0.133	0.025
FAO function for ATP production	0.130	0.367	0.131	**−0.298***	−0.021	−0.111
Glycolytic function						
Glycolysis	−0.034	0.046	0.244	**−0.316***	−0.120	−0.229
Glycolytic capacity	0.010	0.116	0.220	**−0.290***	−0.101	−0.223
Glycolytic reserve	−0.147	**0.618***	0.055	−0.095	0.129	−0.122
Glycolytic reserve (%)	−0.075	**0.620***	0.030	0.046	0.214	−0.011
Mitochondrial function						
Basal respiration	−0.089	0.180	0.102	**−0.272***	0.166	0.125
ATP production	0.023	0.188	0.077	**−0.263***	0.214	0.164
Maximal respiration	0.035	0.134	0.027	−0.210	0.236	0.184
Spare respiratory capacity	0.025	0.061	0.012	−0.096	0.206	0.161
Proton leak	−0.205	0.342	0.151	**−0.266***	0.120	0.043
Coupling efficiency (%)	**0.570***	−0.391	−0.122	0.102	0.068	0.112
ATP production rate						
Total ATP production	0.038	0.096	−0.050	**−0.368****	−0.009	−0.028
Mitochondrial ATP (%)	−0.163	0.063	0.161	−0.078	0.162	**0.358****
Glycolytic ATP (%)	0.163	−0.063	−0.161	0.078	−0.162	**−0.358****

Bold numbers indicate significant correlations.
* $P < 0.05$. ** $P < 0.01$.

identify potential biomarkers of female infertility. Interestingly, the effects of age on GC metabolism were more pronounced in women with ovarian infertility, even though there was no significant difference in the mean age between the two groups (Supplementary Table S1). Specifically, in GC from women with ovarian infertility, there was significant age-associated inhibition of mitochondrial function (reduced maximal respiration and spare respiratory capacity); indicative of an inability to upregulate energy production. Consistent with reduced mitochondrial function, cells from older women with ovarian infertility utilized glycolysis more than oxidative phosphorylation to maintain similar ATP production. Morphological defects and reduced membrane potential have been observed in mitochondria of GCs of older women (≥38 years old) (Tatone *et al.*, 2006; Liu *et al.*, 2017) and are a likely contributor to the functional metabolic changes that we have observed in older ovarian infertility patients.

The Ovarian Infertility patient group also showed a marked association between very high metabolic rates in GCs and failed fertilization. This is clearly visible in the elevated OCR and ECAR readings of women with the worst fertilization rates (n = 10) compared to those with the best fertilization rates (n = 10); see Supplementary Fig. S6G and H. The basis for the elevated GC metabolism in these patients is not known and is an important area of future investigation since this biomarker was correlated with risk of fertilization failure. Importantly, the GC metabolic changes associated with poor fertilization (high FAO, high glycolysis, high basal respiration) are distinct from the changes that occur with aging (namely reduced maximal respiration and coupling efficiency). This high metabolism might be an indication of premature luteinization; and consistent with this, high progesterone on the day of ovulation trigger is associated with poorer fertilization and embryo development outcomes (Woo *et al.*, 2022). Mitochondrial metabolic substrate utilization in GCs can also be negatively influenced by increased FSH dosage (Kordus *et al.*, 2020). Thus, the metabolic alterations in this cohort could be influenced by age, their hormonal treatments, and potentially lifestyle factors.

Correlations between GC metabolism and successful embryo development were also identified, offering insight into the mechanisms by which follicular cells support oocyte developmental competence. Prior to the LH surge, oocytes and GC are directly linked via extensive syncytial connections and through cumulus cell transzonal projections (Kidder and Mhawi, 2002; Clarke, 2022). That GC mitochondrial coupling efficiency is positively correlated with successful fertilization indicates that intercellular communication is intact and mitochondria are functioning appropriately in somatic cells and in oocytes where optimal mitochondrial membrane potential is essential for completion of meiosis and 2-cell formation (Van Blerkom, 2011). The positive association between GC glycolytic reserve and Day 3 development suggests that carbohydrate storage in follicular somatic cells influences the deposition of energy stores to the oocyte as well. Interestingly, FAO was not significantly associated with IVF outcomes, suggesting that this form of metabolism in GCs might primarily influence luteal cell biology rather than directly influence oocyte quality. The relatively late induction of FAO (compared to glycolysis) in mouse GCs (see Fig. 1) supports this concept. A limitation is that there were fewer participants in the Normal Ovarian Function group, and thus additional larger studies are warranted to build upon these foundational data. Importantly, in women with ovarian infertility, there was a strong positive correlation between the relative amount of ATP produced from mitochondria and blastocyst formation rates. This suggests that, despite challenges in the earlier stages of fertilization, when GCs have the functional capacity to obtain more ATP from mitochondria, oocyte developmental competence is more likely to reach the blastocyst stage.

Somewhat surprisingly, increased BMI in women had a relatively modest impact on GC metabolism. This result is different from observations in the obese mouse model which exhibits hyperinsulinemia and mild hyperglycemia (Wu *et al.*, 2015; Umehara *et al.*, 2022), and where multiple aspects of mitochondrial respiration were impaired with obesity. This suggests that significant metabolic disorders (for instance insulin resistance)

were adequately managed in the obese women. Further, although the size of the patient cohort did not permit an analysis of aging and obesity combined, the mouse models clearly show that obesity compounds the effects of aging, leading to severe metabolic dysfunction in GCs that likely contributes to impaired ovulation and/or P4 production as occurs in obese women (Rich-Edwards *et al.*, 2002; Jain *et al.*, 2007).

A strength of our study is that we used mouse models which, although having some metabolic differences to humans (for instance in microbiome-produced metabolites), enabled hormonal responses to be tightly controlled and examined at distinct timepoints. We demonstrate that a diverse range of metabolic pathways are acutely upregulated by ovulatory hCG. Interestingly, we did not detect any significant differences in metabolism between GCs collected 24-h post-PMSG (a mid-point of folliculogenesis with most follicles at the small antral stage) and at 48-h post-PMSG when the preovulatory follicle is fully formed and poised to respond to the LH surge. A previous genome-wide analysis found that glycolysis- and oxidative phosphorylation-related genes are induced, albeit modestly, between 24- and 48-h post-PMSG (Chen *et al.*, 2020). Thus, it is possible that we did not observe metabolic regulation during this phase of folliculogenesis because it is subtle and masked by the magnitude of the hCG-induced metabolic changes; or alternatively, gene expression changes may not manifest as functional metabolic shifts until after the LH surge. Cell type-specific regulation was also observed. Specifically, in mouse GCs, glycolysis was upregulated within 8 h following hCG, while both long-chain FAO and mitochondrial respiration were induced by 12-h post-hCG. In contrast, in COCs, mitochondrial respiration and glycolysis were more rapidly increased (within 4 h following ovulatory hCG); and then downregulated within the next 4–8 h. These distinct metabolic profiles likely reflect the vastly different functions and fates of the two cell types. GCs respond to ovulatory hCG by increasing multiple aspects of cellular metabolism, concurrent with terminal differentiation into large lipid-laden luteal cells, which have the capacity to remain viable and secrete progesterone through the entirety of a resulting pregnancy. In contrast, although cumulus cells produce matrix proteins and progesterone which are essential for sperm chemotaxis and binding; following ovulation cumulus cells are relatively short-lived and do not persist long beyond the expected time of fertilization (Russell and Robker, 2018). COCs have a more moderate metabolic profile compared to GCs; however, they still exhibit a burst of metabolic activity at 4-h post-hCG, concurrent with the massive induction of cumulus matrix production and a migratory phenotype (Akison *et al.*, 2012). The fact that cumulus cell metabolism near the time of ovulation is not reflective of the functional peak, suggests that measuring cumulus cell metabolism at the time of oocyte pick-up may be too late to identify metabolic markers of oocyte quality in these cells. Importantly however, mitochondrial membrane potential in cumulus cells was found to be positively correlated with the number of MII oocytes retrieved (Dumesic *et al.*, 2016), suggesting that cumulus cell metabolism influences earlier stages of follicular growth and oocyte maturation.

In summary, this study reveals the dynamic changes in energy metabolism in GCs and how these parameters deviate in infertility patients, especially with aging. By uncovering the specific metabolic perturbations associated with poor oocyte quality, this new understanding of the links between GC metabolism and subsequent embryonic development can direct new therapeutic strategies focused on optimizing mitochondrial metabolism.

Supplementary data

Supplementary data are available at *Human Reproduction* online.

Data availability

The data underlying this article will be shared on reasonable request to the corresponding author.

Acknowledgements

Dr Macarena Gonzalez and Haley Connaughton provided expert advice and technical support. Brent Neumann and Julian Heng (Remotely Consulting, Australia) provided professional English-language scientific editing of this article (Manuscript Certificate No. 0Zq8Am5S).

Authors' roles

A.M., R.D.R., T.U., and R.L.R. designed the study. The experiments were performed by A.M., K.M.S., D.T.D., T.U., and Y.E.W. Data analysis was performed by A.M., R.D.R., T.U., and R.L.R. The manuscript was drafted by A.M., R.D.R., K.M.S., and R.L.R., with editorial contributions from D.T.D., Y.E.W., and D.L.R. Supervision was provided by H.S., D.L.R., and R.L.R.

Funding

National Health and Medical Research Council of Australia (APP1165633 to R.L.R.).

Conflict of interest

The authors have no conflicts of interest of relevance to this study.

References

Aardema H, Vos PL, Lolicato F, Roelen BA, Knijn HM, Vaandrager AB, Helms JB, Gadella BM. Oleic acid prevents detrimental effects of saturated fatty acids on bovine oocyte developmental competence. *Biol Reprod* 2011;**85**:62–69.

Akison LK, Alvino ER, Dunning KR, Robker RL, Russell DL. Transient invasive migration in mouse cumulus oocyte complexes induced at ovulation by luteinizing hormone. *Biol Reprod* 2012;**86**:125.

Andreas E, Winstanley YE, Robker RL. Effect of obesity on the ovarian follicular environment and developmental competence of the oocyte. *Curr Opin Endocr Metab Res* 2021;**18**:152–158.

Arsov T, Silva DG, O'Bryan MK, Sainsbury A, Lee NJ, Kennedy C, Manji SS, Nelms K, Liu C, Vinuesa CG *et al.* Fat aussie—a new Alström syndrome mouse showing a critical role for ALMS1 in obesity, diabetes, and spermatogenesis. *Mol Endocrinol* 2006;**20**:1610–1622.

Babayev E, Duncan FE. Age-associated changes in cumulus cells and follicular fluid: the local oocyte microenvironment as a determinant of gamete quality. *Biol Reprod* 2022;**106**:351–365.

Bartolacci A, Buratini J, Moutier C, Guglielmo MC, Novara PV, Brambillasca F, Renzini MM, Dal Canto M. Maternal body mass index affects embryo morphokinetics: a time-lapse study. *J Assist Reprod Genet* 2019;**36**:1109–1116.

Broekmans FJ, Soules MR, Fauser BC. Ovarian aging: mechanisms and clinical consequences. *Endocr Rev* 2009;**30**:465–493.

Chen Y, Wang X, Yang C, Liu Q, Ran Z, Li X, He C. A mouse model reveals the events and underlying regulatory signals during the

gonadotrophin-dependent phase of follicle development. *Mol Hum Reprod* 2020;**26**:920–937.

Clarke HJ. Transzonal projections: essential structures mediating intercellular communication in the mammalian ovarian follicle. *Mol Reprod Dev* 2022;**89**:509–525.

Comstock IA, Kim S, Behr B, Lathi RB. Increased body mass index negatively impacts blastocyst formation rate in normal responders undergoing in vitro fertilization. *J Assist Reprod Genet* 2015; **32**:1299–1304.

Cordeiro FB, Montani DA, Pilau EJ, Gozzo FC, Fraietta R, Turco EGL. Ovarian environment aging: follicular fluid lipidomic and related metabolic pathways. *J Assist Reprod Genet* 2018;**35**:1385–1393.

Dogan B, Karaer A, Tuncay G, Tecellioglu N, Mumcu A. High-resolution (1)H-NMR spectroscopy indicates variations in metabolomics profile of follicular fluid from women with advanced maternal age. *J Assist Reprod Genet* 2020;**37**:321–330.

Dumesic DA, Guedikian AA, Madrigal VK, Phan JD, Hill DL, Alvarez JP, Chazenbalk GD. Cumulus cell mitochondrial resistance to stress in vitro predicts oocyte development during assisted reproduction. *J Clin Endocrinol Metab* 2016;**101**:2235–2245.

Dumesic DA, Meldrum DR, Katz-Jaffe MG, Krisher RL, Schoolcraft WB. Oocyte environment: follicular fluid and cumulus cells are critical for oocyte health. *Fertil Steril* 2015;**103**:303–316.

Dunning KR, Cashman K, Russell DL, Thompson JG, Norman RJ, Robker RL. Beta-oxidation is essential for mouse oocyte developmental competence and early embryo development. *Biol Reprod* 2010;**83**:909–918.

Esencan E, Simsek B, Seli E. Analysis of female demographics in the United States: life expectancy, education, employment, family building decisions, and fertility service utilization. *Curr Opin Obstet Gynecol* 2021;**33**:170–177.

Flurkey K, Currer JM, Harrison DE. Mouse models in aging research. In: Fox JG, Barthold S, Davisson M, Newcomer CE, Quimby FW, Smith A (eds). *The Mouse in Biomedical Research*. New York: Elsevier, 2007,637–672.

Gardner DK. In-vitro culture of human blastocysts. *Towards reproductive certainty: fertility and genetics beyond 1999* 1999: 378-388.

Gonzalez MB, Robker RL, Rose RD. Obesity and oocyte quality: significant implications for ART and emerging mechanistic insights. *Biol Reprod* 2022;**106**:338–350.

Harlow CR, Winston RM, Margara RA, Hillier SG. Gonadotrophic control of human granulosa cell glycolysis. *Hum Reprod* 1987; **2**:649–653.

Heydet D, Chen LX, Larter CZ, Inglis C, Silverman MA, Farrell GC, Leroux MR. A truncating mutation of Alms1 reduces the number of hypothalamic neuronal cilia in obese mice. *Dev Neurobiol* 2013; **73**:1–13.

Jain A, Polotsky AJ, Rochester D, Berga SL, Loucks T, Zeitlian G, Gibbs K, Polotsky HN, Feng S, Isaac B *et al.* Pulsatile luteinizing hormone amplitude and progesterone metabolite excretion are reduced in obese women. *J Clin Endocrinol Metab* 2007;**92**:2468–2473.

Kidder GM, Mhawi AA. Gap junctions and ovarian folliculogenesis. *Reproduction* 2002;**123**:613–620.

Kordus RJ, Hossain A, Malter HE, LaVoie HA. Mitochondrial metabolic substrate utilization in granulosa cells reflects body mass index and total follicle stimulating hormone dosage in in vitro fertilization patients. *J Assist Reprod Genet* 2020;**37**:2743–2756.

Leary C, Leese HJ, Sturmey RG. Human embryos from overweight and obese women display phenotypic and metabolic abnormalities. *Hum Reprod* 2015;**30**:122–132.

Li G, Vega R, Nelms K, Gekakis N, Goodnow C, McNamara P, Wu H, Hong NA, Glynne R. A role for Alström syndrome protein, alms1, in kidney ciliogenesis and cellular quiescence. *PLoS Genet* 2007; **3**:e8.

Liu Y, Han M, Li X, Wang H, Ma M, Zhang S, Guo Y, Wang S, Wang Y, Duan N *et al.* Age-related changes in the mitochondria of human mural granulosa cells. *Hum Reprod* 2017;**32**:2465–2473.

Pacella L, Zander-Fox DL, Armstrong DT, Lane M. Women with reduced ovarian reserve or advanced maternal age have an altered follicular environment. *Fertil Steril* 2012;**98**:986–994.e1-2.

Paczkowski M, Schoolcraft WB, Krisher RL. Fatty acid metabolism during maturation affects glucose uptake and is essential to oocyte competence. *Reproduction* 2014;**148**:429–439.

Pantasri T, Wu LL, Hull ML, Sullivan TR, Barry M, Norman RJ, Robker RL. Distinct localisation of lipids in the ovarian follicular environment. *Reprod Fertil Dev* 2015;**27**:593–601.

Park JY, Su YQ, Ariga M, Law E, Jin SL, Conti M. EGF-like growth factors as mediators of LH action in the ovulatory follicle. *Science* 2004;**303**:682–684.

Peng XR, Hsueh AJ, LaPolt PS, Bjersing L, Ny T. Localization of luteinizing hormone receptor messenger ribonucleic acid expression in ovarian cell types during follicle development and ovulation. *Endocrinology* 1991;**129**:3200–3207.

Plewes MR, Krause C, Talbott HA, Przygrodzka E, Wood JR, Cupp AS, Davis JS. Trafficking of cholesterol from lipid droplets to mitochondria in bovine luteal cells: acute control of progesterone synthesis. *FASEB J* 2020;**34**:10731–10750.

Przygrodzka E, Plewes MR, Davis JS. Luteinizing hormone regulation of inter-organelle communication and fate of the corpus luteum. *Int J Mol Sci* 2021;**22**:9972.

Richani D, Dunning KR, Thompson JG, Gilchrist RB. Metabolic co-dependence of the oocyte and cumulus cells: essential role in determining oocyte developmental competence. *Hum Reprod Update* 2021;**27**:27–47.

Rich-Edwards JW, Spiegelman D, Garland M, Hertzmark E, Hunter DJ, Colditz GA, Willett WC, Wand H, Manson JE. Physical activity, body mass index, and ovulatory disorder infertility. *Epidemiology* 2002;**13**:184–190.

Robker RL, Akison LK, Bennett BD, Thrupp PN, Chura LR, Russell DL, Lane M, Norman RJ. Obese women exhibit differences in ovarian metabolites, hormones, and gene expression compared with moderate-weight women. *J Clin Endocrinol Metab* 2009;**94**:1533–1540.

Russell DL, Robker RL. Cumulus cells. In: Skinner MK (ed). *Encyclopedia of Reproduction*, 2nd edn. Academic Press, Elsevier, 2018,42–46. https://doi.org/10.1016/B978-0-12-801238-3.64392-1.

Sanchez-Lazo L, Brisard D, Elis S, Maillard V, Uzbekov R, Labas V, Desmarchais A, Papillier P, Monget P, Uzbekova S. Fatty acid synthesis and oxidation in cumulus cells support oocyte maturation in bovine. *Mol Endocrinol* 2014;**28**:1502–1521.

Schmidt CA, Fisher-Wellman KH, Neufer PD. From OCR and ECAR to energy: perspectives on the design and interpretation of bioenergetics studies. *J Biol Chem* 2021;**297**:101140.

Tatone C, Carbone MC, Falone S, Aimola P, Giardinelli A, Caserta D, Marci R, Pandolfi A, Ragnelli AM, Amicarelli F. Age-dependent changes in the expression of superoxide dismutases and catalase are associated with ultrastructural modifications in human granulosa cells. *Mol Hum Reprod* 2006;**12**:655–660.

Umehara T, Winstanley YE, Andreas E, Morimoto A, Williams EJ, Smith KM, Carroll J, Febbraio MA, Shimada M, Russell DL *et al.* Female reproductive life span is extended by targeted removal of fibrotic collagen from the mouse ovary. *Sci Adv* 2022;**8**:eabn4564.

Valckx SD, Arias-Alvarez M, De Pauw I, Fievez V, Vlaeminck B, Fransen E, Bols PE, Leroy JL. Fatty acid composition of the follicular fluid of normal weight, overweight and obese women undergoing assisted reproductive treatment: a descriptive cross-sectional study. *Reprod Biol Endocrinol* 2014;**12**:13.

Valckx SD, De Pauw I, De Neubourg D, Inion I, Berth M, Fransen E, Bols PE, Leroy JL. BMI-related metabolic composition of the

follicular fluid of women undergoing assisted reproductive treatment and the consequences for oocyte and embryo quality. *Hum Reprod* 2012;**27**:3531–3539.

Van Blerkom J. Mitochondrial function in the human oocyte and embryo and their role in developmental competence. *Mitochondrion* 2011;**11**:797–813.

Van Hoeck V, Leroy JL, Arias Alvarez M, Rizos D, Gutierrez-Adan A, Schnorbusch K, Bols PE, Leese HJ, Sturmey RG. Oocyte developmental failure in response to elevated nonesterified fatty acid concentrations: mechanistic insights. *Reproduction* 2013;**145**:33–44.

Woo J, Kwon H, Choi D, Park C, Kim J, Shin J, Kim J, Kang YJ, Koo H. Effects of elevated progesterone levels on the day of hCG on the quality of oocyte and embryo. *J Clin Med* 2022; **11**:4319.

Wu LL, Russell DL, Wong SL, Chen M, Tsai TS, St John JC, Norman RJ, Febbraio MA, Carroll J, Robker RL. Mitochondrial dysfunction in oocytes of obese mothers: transmission to offspring and reversal by pharmacological endoplasmic reticulum stress inhibitors. *Development* 2015; **142**:681–691.

Human Reproduction, 2024, 39, 2053–2066
https://doi.org/10.1093/humrep/deae154
Original Article